Effect of gallium loading on the hydrodesulfurization activity of unsupported Ga$_2$S$_3$/WS$_2$ catalysts

T.A. Zepeda [a,*], B. Pawelec [b], J.N. Díaz de León [a], J.A. de los Reyes [c], A. Olivas [a]

[a] *Centro de Nanociencias y Nanotecnología – UNAM, Km. 107 Carretera Tijuana-Ensenada, CP. 22800, Ensenada, B.C., Mexico*
[b] *Instituto de Catálisis y Petroleoquímica, CSIC, c/Marie Curie 2, Cantoblanco, 28049 Madrid, Spain*
[c] *Área de Ingeniería Química, Universidad Autónoma Metropolitana-Iztapalapa, Iztapalapa, 09340, D.F., Mexico*

ABSTRACT

The effect of gallium incorporation into unsupported tungsten sulfide catalysts was investigated in dibenzothiophene (DBT) hydrodesulfurization (HDS) reaction. The Ga/WS$_2$ catalysts with variable gallium loadings (0.5–2.5 wt%) were prepared by decomposition of W-thiosalt followed by impregnation with the Ga salt precursor. The samples were characterized by a variety of techniques: ICP-AES, N$_2$ adsorption–desorption at −196 °C, XRD, SEM, XPS, FTIR of CO chemisorbed and TPD-NH$_3$. The last two techniques showed that gallium addition has a strong effect on the morphology of the tungsten sulfide phase by modifying the coordinately unsaturated sites (CUS) of the WS$_2$ phase and total catalyst acidity. The HDS of DBT reaction (T = 320 °C, P_{H_2} = 5.5 MPa) was found to proceed through two main parallel pathways: hydrogenation (HYD) and direct desulfurization (DDS), the latter being the main reaction route. With respect to Ga-free WS$_2$ sample, all Ga-loaded catalysts showed an increase of HDS activity via hydrogenation (HYD) pathway and additional DBT cracking. The 1.5% Ga/WS$_2$ catalyst was the most active among the catalysts studied. On the basis of the catalyst structure–activity relationship, this was linked to a homogeneous distribution of Ga species on the surface of WS$_2$ (SEM), the largest amount of acid sites (from TPD-NH$_3$) and the largest amount of "corner sites" on the WS$_2$ slabs determined by FTIR-CO. For the Ga-containing catalysts, an increase of DBT transformation via HYD route was explained in terms of the formation of new CUS sites on WS$_2$ phase as well as to an increase of the catalyst acidity. Acidity is a key requirement influencing on DBT cracking.

© 2011 Elsevier B.V. All rights reserved.

1. Introduction

Owing to environmental and clean-fuel legislation limiting sulfur content in diesel to the ultra-low level (<10 ppm of S), the deep hydrodesulfurization (HDS) of petroleum streams has been the focus of many studies [1–3 and references within]. Transition metal sulfides (TMS) supported on a high surface area γ-Al$_2$O$_3$ employed by refiners are not effective for deep hydrodesulfurization. Thus, the challenge is to engineer novel and more effective catalysts for the deep HDS of petroleum streams [1,2].

In the new generation of hydrotreating catalysts, four approaches are mainly used: (i) the variation of the active phase; (ii) the substitution of γ-Al$_2$O$_3$ by other carriers [4–12]; (iii) the modification of alumina with additives such as boron, fluorine or phosphorous [13,14], and (iv) the use of unsupported catalysts [15–20]. Concerning the latter, it was found that unsupported

Ni–Mo–W sulfide catalysts exhibited at least 3 times higher activity than the commercial alumina-supported NiMo and CoMo catalysts [19]. The best results were achieved with the unsupported NEBULA catalysts, developed jointly by Akzo Nobel, Nippon Ketjen and Exxon Mobil in 2001 [20]. This improvement of activity was explained as due to the appropriate combination of transition metals (Ni, Mo and W in a sulfided forms) and the final arrangement of atoms at the border of crystallites. Among different preparation procedure of the unsupported HDS catalysts the thiosalt decomposition seems to be most interesting method because it provides a simple and reproducible method for obtaining Mo(W)S$_2$ catalysts [21–24]. Since the thiosalts have already sulfur bond to the metal atoms in a tetrahedral coordination, the main advantage of the use of this catalyst preparation method resides in the fact that it avoids the complex oxide–sulfide transformation which often leads to a partial sulfidation of Mo(W)O$_3$ species and therefore to lower HDS activity [24].

As compared with Mo-based HDS catalysts [2], their W-based counterparts are much less studied [25–29]. This is probably because WO$_3$ species are more difficult to reduce than MoO$_3$

[30,31]. However, the reducibility of tungsten species could be improved by incorporation of promoters [28] and/or by using thiosalt precursors [21–24]. The effect of the catalyst preparation method was studied by Pedraza et al. [32] who found that catalyst preparation through the decomposition of thiosalts impregnated with the promoter (DTI) was more effective in terms of the catalytic activity than the homogeneous sulfide co-precipitation (HSP) method. The enhancement in catalytic activity was attributed to an ameliorated dispersion of the promoter in WS_2, which was preserved during the gradual decomposition of the complex. Indeed, by using the classical impregnation method and Co(Ni) nitrate as precursors, the promoter has a tendency to be sulfided before molybdenum and tungsten and to form isolated sulfide particles Co_9S_8 or Ni_3S_2 which are quite inactive for HDS reaction [33–35]. On the contrary, the introduction of promoter directly onto a metal sulfide leads to well-promoted catalysts with high potential for industrial applications, as it was recently demonstrated for supported Mi–MoS_2 catalysts [36].

Recently, alumina modified with gallium has emerged as an interesting substrate for supporting Ni(Co)Mo hydrotreating (HDT) catalysts [37–41]. The mixed Ga_2O_3–Al_2O_3 oxide prepared by co-precipitation has been used also for supporting CoMo catalysts [42]. To the best of our knowledge, the effect of gallium as promoter was studied only by Park and Rhee [43] who observed that gallium introduced to the GaNiMo/Al_2O_3 catalysts as a secondary promoter enhanced the catalytic activity in reaction of hydrodenitrogenation (HDN). In general, the enhancement of the catalyst activity after Ga incorporation onto alumina support was linked with the higher affinity Ga^{3+} ions for surface tetrahedral Al^{3+} sites with respect to the Ni^{2+} (or Co^{2+}) ions leading to inhibition of the formation of inactive $NiAl_2O_4$ (or $CoAl_2O_4$) phases [37–41]. Similarly, the addition of optimized amount of Ga (1.2 wt%) onto alumina support led to the enhancement of the activity of NiMo/Ga/γ-Al_2O_3 catalyst in the HDS of DBT and 4,6-DMDBT without modifying its initial textural properties [40]. This was attributed to the occupation of tetrahedral sites by gallium, resulting in an increase in the amount of nickel species that can participate in the decoration of MoS_2 slabs by forming "Ni–Mo–S" phase [40]. Additionally, the presence of Ga led to an enhancement of Mo sulfidation degree and inhibition of the formation of $NiAl_2O_4$ phase [39,40]. Díaz de León et al. [41] studied the effect of gallium incorporation into monometallic W/γ-Al_2O_3 catalysts on their catalytic response in the HDS of DBT. It was found that the gallium incorporation had a strong effect in the formation of tungsten species at the surface of the catalysts. Higher activity was found for the W/γ-Al_2O_3 sample with 1.09 wt% of Ga, this was related with the high dispersion of W species in this sample and the superior amount of coordinately unsaturated sites. Olorunyolemi and Kydd [42] used mixed Ga_2O_3–Al_2O_3 oxides for supporting CoMo HDS catalysts. These authors found that, contrary to the Al_2O_3 alone, the hybrid gallium–aluminium oxides were found to be active in cumene cracking [42]. This result strongly suggests that cracking might occur on Lewis Ga^{3+} acid sites.

To the best of our knowledge, the effect of gallium addition into unsupported WS_2 catalysts is not yet reported in the literature. Moreover, there is still no clear role of gallium as additive in the formulation of hydrodesulfurization catalysts. In particular, it is not clear whether the gallium acts as promoter and/or only causes significant changes in the electronic and morphological properties of the supported catalysts or decreases the formation of promoter-Al_2O_3 phase. This prompts us to prepare Ga-loaded unsupported WS_2 catalysts by decomposition of thiosalt impregnated with promoter in order to investigate the role of gallium in binary Ga/WS_2 catalysts. The catalytic systems were characterized by several physico-chemical techniques (ICP-AES, S_{BET}, XRD, SEM, XPS, FTIR-CO chemisorbed and NH_3-TPD) and tested in HDS of DBT

performed in a batch reactor at 320 °C and hydrogen pressure of 5.5 MPa.

2. Experimental

2.1. Catalyst preparation

The unsupported WS_2 samples were prepared following the procedure described elsewhere [44]. An aqueous solution of ammonium metatungstate ((NH_4)$_6$$H_2$$W_{12}$$O_{40}$·$xH_2O$, Aldrich 98%) and ammonium hydroxide (NH_4OH, solution 10%) was bubbled with hydrogen sulfide at 400 °C for 4 h. Afterwards, the reaction vessel was kept in an ice bath to precipitate yellow ammonium thiotungstate. The obtained crystals were filtered and kept in sealed containers under argon atmosphere. Binary Ga/WS_2 samples were prepared by adding drop-wise to ammonium thiotungstate crystals an acetone solution of gallium nitrate hydrate (Ga(NO_3)$_3$·xH_2O, Aldrich 99%) in the appropriate amount to yield 0.5, 1.5 and 2.5 wt% Ga-loaded catalysts (successive precipitation method). The solution mixture was stirred at 40 °C for 3 h, until the solvent was evaporated. Then, the Ga-free and Ga-containing samples were decomposed to tungsten disulfide by heating to 400 °C for 6 h under a residual pressure of 10^{-4} mbar. The samples were stored under nitrogen atmosphere with the aim to avoid contact with air. Before reaction, the dried samples were treated at 450 °C in hydrogen sulfide/hydrogen gas mixture (20 vol. % H_2S) with flow of 80 mL/min for 6 h, reaching this temperature in 3 h. The Ga-containing catalysts were labeled as $x\%$ Ga/WS_2 where $x\%$ denotes the nominal gallium content (wt%).

2.2. Characterization methods

2.2.1. Chemical analyses

The metal loadings of the sulfided catalysts were determined by Inductively Coupled Plasma Atomic Emission Spectroscopy (ICP-AES), Perkin Elmer Optima 3300DV. The solid samples were first digested (in a mixture of HF, HCl and HNO_3) in a microwave oven for 2 h.

2.2.2. Textural parameters

The textural properties of the reduced catalysts (under 60 mL/min of hydrogen flow at 350 °C for 2 h) were determined from the adsorption–desorption isotherms of nitrogen at −196 °C, recorded with a Micromeritics TriStar 3000 apparatus. Prior to the experiments, the samples were degassed at 270 °C in vacuum for 5 h. The volume of the adsorbed N_2 was normalized to the standard temperature and pressure. The specific areas of the samples were calculated by applying the BET method to the nitrogen adsorption data within the 0.005–0.25 P/P^0 range.

2.2.3. X-ray diffraction

The X-ray diffraction (XRD) measurements of the sulfided samples were made in a Philips spectrometer model X'pert using the Cu Kα radiation (40 kV, 30 mA) with wavelength of 0.154 nm. Interpretation of XRD data was made by comparing experimental patterns with those reported in the ICDD-PDF data bases.

2.2.4. Scanning electron microscopy (SEM)

The catalysts morphology was studied by SEM in a Jeol 5300 scanning electron microscope with a depressive energy detector (EDS).

2.2.5. X-ray photoelectron spectroscopy (XPS)

A RIBER LDM-32 XPS instrument equipped with a hemispherical electron analyzer and a Mg Kα ($h\nu$ = 1253.6 eV) X-ray source was used. The samples were first placed in a copper holder mounted

on a sample-rod in the pretreatment chamber of the spectrometer and then outgassed at 130 °C for 1 h before transfer to the analysis chamber. All catalysts were outgassed at 10^{-5} mbar and then transferred to the ion-pumped analysis chamber, where residual pressure was kept below 1×10^{-9} mbar during data acquisition. The binding energies (BE) were referenced to the C 1s peak (284.9 eV) to account for the charging effects. The areas of the peaks were computed after fitting of the experimental spectra to Gaussian/Lorentzian curves and removal of the background (Shirley function). Surface atomic ratios were calculated from the peak area ratios normalized by the corresponding atomic sensitivity factors.

2.2.6. FTIR of chemisorbed CO

The samples were sulfided *in situ*, at atmospheric pressure, with a 20% H_2S/H_2 at 450 °C with a flow of 80 mL/min for 6 h, reaching this temperature in 3 h. The sample was then degassed under 10^{-5} mbar at 450 °C for 1 h. Then, CO adsorption was performed at low temperature, approximately at −100 °C, in order to avoid reaction with the catalyst surface. Small calibrated doses of CO were introduced in the IR cell up to an equilibrium pressure of approximately 7 mbar. Subsequent, the CO was evacuated at low temperature (−100 °C) up to a residual pressure of 10^{-5} mbar, and finally the FTIR was recorded on Bruker model Tensor 27 spectrophotometer at a resolution of 4 cm^{-1}.

2.2.7. TPD-NH$_3$ measurements

The acidity of the sulfided catalysts was determined by TPD-NH$_3$ measurements using an Altamira TPD/TPR device. 0.05 g of sulfide samples were first degassed in a He flow (Air Liquide, 99.996%) at 200 °C for 1 h. Then, the samples were saturated with a mixture of 10% NH_3/He stream at 100 °C for 25 min. The physically adsorbed NH_3 was then removed by treatment in a He flow for 30 min at 80 °C. The ammonia desorption was performed from 50 °C to 700 °C using a He flow and heating rate of 15 °C min^{-1}, while recording TCD signal.

2.2.8. Catalytic activity

The catalysts were sulfided in a U-shaped glass flow reactor. First the sample was flushed in a nitrogen flow gradually increasing the temperature up to 150 °C and then switching to the sulfidation mixture (H_2/H_2S 20 vol. % H_2S) at a flow of 80 mL/min and increasing the temperature up to 450 °C for 6 h, reaching this temperature within 2.5 h. The sulfidation was carried out at this temperature for 6 h. Then the sample was cooled down to room temperature, changing the sulfidation mixture to nitrogen when the temperature had decreased to 150 °C. The sulfided sample was transferred to the reactor in an argon atmosphere with the aim to avoid contact with air.

The catalytic activity in the reaction of HDS of DBT was measured in a batch Parr reactor charged around 0.2 g of the catalyst and around 0.3 g of DBT dissolved in 100 mL of *n*-hexadecane. The reactor was additionally purged with nitrogen to eliminate traces of oxygen. The reaction was carried out at 320 °C for 6 h under hydrogen pressure of 5.5 MPa. The external diffusion limitations was excluded, checked by varying amount of catalyst and the power of stirring (1000, 800 and 700 rpm). In order to minimise internal diffusion limitations, all catalysts were thoroughly ground to a fine powder. The heat-up time of the reactor to the reaction temperature was 35 min. The reaction products were analyzed by GC on a Perkin-Elmer XL equipment using a 30 m long Altech econo capillary column.

Table 1
Gallium content[a], textural properties[b] and acidity[c] of the bulk WS_2 and sulfided Ga/WS_2 bulk catalysts.

Catalysts	Ga (wt%)	S_{BET} (m^2 g^{-1})	V_p (cm^3 g^{-1})	Acid sites (mmol$_{NH_3}$ g$_{cat}^{-1}$)
WS_2	0	22	0.08	0.014
0.5% Ga/WS_2	0.46	38	0.10	0.015
1.5% Ga/WS_2	1.37	55	0.12	0.018
2.5% Ga/WS_2	2.42	64	0.13	0.025

[a] As determined by ICP-AES technique.
[b] Specific BET surface area (S_{BET}) and total pore volume (V_p) as determined by N_2 adsorption desorption measurements at −196 °C.
[c] Calculated from area of 1st peak of TPD-NH$_3$ profiles.

3. Results and discussion

3.1. Chemical and textural properties of sulfide catalysts

In this study, bulk WS_2 catalyst with a high specific area was prepared via thermal decomposition of the ammonium thiotungstate compound whereas Ga/WS_2 catalysts were prepared by decomposition of thiosalt impregnated with promoter. The gallium content achieved after sulfidation of the Ga-containing catalysts was close to the nominal one (Table 1).

The values of the specific BET surface area (S_{BET}) and pore volume of the bulk WS_2 and sulfided Ga/WS_2 catalysts are compiled in Table 1. Incorporation of gallium on the Ga/WS_2 bulk catalysts led to an increase of the values of both parameters with respect to the Ga-free WS_2 sample: the S_{BET} from 22 to 64 m^2 g^{-1} and the pore volume from 0.08 to 0.13 cm^3 g^{-1}. Considering SEM images of the catalysts (*vide infra*), the possible explanation of this increase is that the introduction of gallium onto the WS_2 disrupts the porous structure of bulk WS_2 catalyst slightly, creating small pores. Although for both textural parameters the observed trend is: 2.5% Ga/WS_2 > 1.5% Ga/WS_2 > 0.5% Ga/WS_2 > WS_2, one may note that this increase is not linear with an increase of the Ga loading.

The scanning electron micrographs (SEM) provide useful information for understanding the textural differences between the Ga/WS_2 and bulk WS_2 samples. The SEM micrographs of the Ga-containing catalysts are shown in Fig. 1. The SEM images indicate that the particles in the samples have a disordered morphology and compact shape. The WS_2 sample shows the agglomerates with a larger size (Fig. 1(a)) with respect to the Ga-containing samples, which have agglomerates around 10–20 mm (Fig. 1(b)–(d)). Thus, one might conclude that the decomposition of thiosalt impregnated with promoter followed by sulfidation led to the formation of smaller agglomerates than in case of WS_2 catalyst prepared by decomposition of ammonium thiotungstate.

3.2. Wide-angle X-ray diffraction (XRD)

Wide-angle XRD profiles were recorded with the aim to investigate the presence of any crystallite species in the catalysts. The X-ray diffraction patterns of the sulfided Ga/WS_2 samples are shown in Fig. 2. As seen in this figure, all catalysts show peaks at 2θ values at approximately 14.4° and 33.6° which are characteristics of (0 0 2) and (1 0 1) planes, respectively, of hexagonal WS_2 phase (JCPDS-ICDD 01-084-1398). With exception of the 2.5% Ga/WS_2 sample having highest Ga loading, all catalysts show a peak at 41.4°, which is associated with the plane (1 2 0) of the WO_3 phase (JCPDS-ICDD 01-086-0134). The presence of this phase confirms that WO_3 particles are first reduced to WO_{3-x} (x = 1 and 2), followed by conversion into hexagonal layered WS_2 [45]. Thus, the presence of gallium had positive effect on the sulfidation degree of tungsten oxide species. The average particle size from XRD patterns was calculated by the Debye–Scherrer equation using the
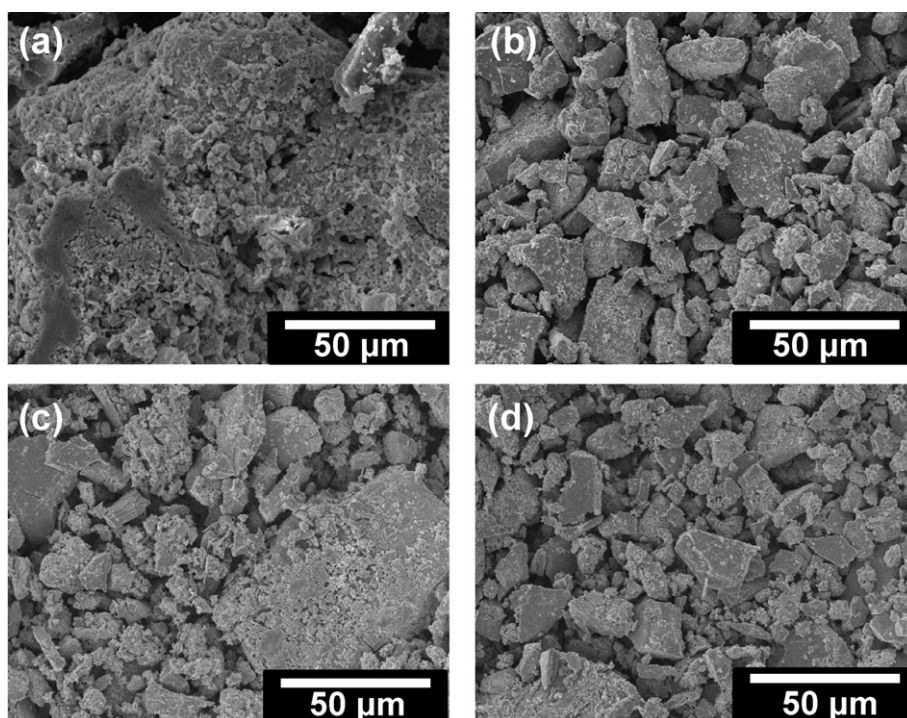
Fig. 1. SEM images of the unsupported catalysts: (a) WS_2, (b) 0.5% Ga/WS_2, (c) 1.5% Ga/WS_2 and (d) 2.5% Ga/WS_2.

lines at $2\theta = 14.2°$ and $33.6°$. The WS_2 crystal size follows the trend: WS_2 (8.7 nm) > 2.5% Ga/WS_2 (5.8 nm) > 1.5% Ga/WS_2 (5.5 nm) > 0.5% Ga/WS_2 (5.0 nm). The Ga-free sample showed the larger WS_2 crystal size (8.7 nm) in comparison with the Ga-containing samples (5.0–5.8 nm) indicating that the incorporation of gallium led to decrease of the size of WS_2 crystals formed upon catalyst sulfidation at 450 °C.

Apart from the tungsten species, all Ga-containing samples record diffraction lines at 2θ values of approximately $28.3°$ and $59.2°$ indicating the presence of Ga_2S_3 crystallites [46]. Additionally, both 1.5% Ga/WS_2 and 2.5% Ga/WS_2 catalysts show a minor diffraction peak at $48.9°$ corresponding to the oxidized Ga^{3+} species (Ga_2O_3 phase) [47]. The average crystal size of Ga_2O_3 species calculated by the Debye–Scherrer equation was 6.0 nm

Fig. 2. X-ray diffractograms of the unsupported catalysts: (a) WS_2, (b) 0.5% Ga/WS_2, (c) 1.5% Ga/WS_2 and (d) 2.5% Ga/WS_2.

(2.5% Ga/WS_2) and 4.1 nm (1.5% Ga/WS_2). The WS_2 crystal size follows the trend: WS_2 (8.7 nm) > 2.5% Ga/WS_2 (5.8 nm) > 1.5% Ga/WS_2 (5.5 nm) > 0.5% Ga/WS_2 (5.0 nm). In summary, results of XRD indicate that the presence of Ga clusters on the surface of the unsupported WS_2 catalyst results in: (i) the enhancement of the sulfidation of tungsten oxide species and (ii) the decrease in WS_2 crystal size. However, the Ga_2O_3 crystal size increases with an increase of Ga content from 1.5 to 2.5 wt%.

3.3. XPS

The XPS spectra provide useful information on the surface species of the sulfided catalysts and their relative proportions. The XP spectra of W 4f and Ga 2p core-levels of the WS_2 and sulfided Ga/WS_2 catalysts are shown in Figs. 3 and 4, respectively. The values of the binding energies (BE) of the W $4f_{7/2}$, Ga $2p_{3/2}$ and S $2p_{3/2}$ are listed in Table 2 along with the Ga/W and S/(W + Ga) atomic ratios. All samples showed an S $2p_{3/2}$ signal at 161.2 eV, which is characteristic of S^{2-} ions [48]. The absence of a BE around 168 eV, where sulfate species are usually observed, indicates that the experimental procedure followed during sulfidation and sample transfer within the spectrometer chamber was efficient in avoiding air contact.

The decomposition of W 4f spectra is well documented in the literature (Fig. 3) [23]. The best fitting of the W 4f profiles was obtained by including two doublets, each one including the $4f_{7/2}$ and $4f_{5/2}$ lines coming from the spin–orbit splitting. For the Ga-free WS_2 sample, the BE's of the two W $4f_{7/2}$ components were found to be around 32.2 and 35.5 eV. According to the literature [23,49–51], the W $4f_{7/2}$ peak at 32.2 eV corresponds to W^{IV} species in a WS_2 structure while the peak at 35.5 eV is typical of the non-sulfided W^{VI} species in WO_3 phase. The proportion of sulfided W species is lower than of oxidized ones (45% vs. 55%) indicating a difficult sulfidation of the unsupported WS_2 catalyst under sulfidation conditions employed (20% H_2S/80% H_2 mixture, 450 °C for 6 h). Contrary to the bulk WS_2 sample, all sulfided Ga/WS_2 catalysts showed a narrow peak with BE close to 32.3 eV,
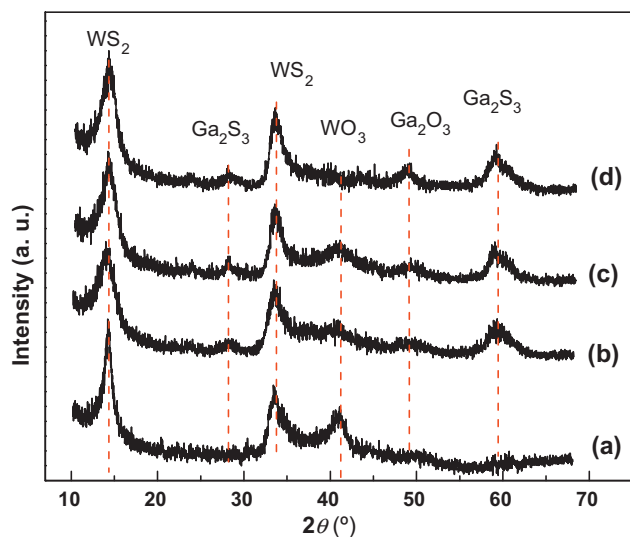
Table 2
Binding energies (eV) of core levels and surface atomic ratios of the bulk WS_2 and sulfided Ga/WS_2 bulk catalysts.

Catalysts	W 4f$_{7/2}$	Ga 2p$_{3/2}$	S 2p	Ga/W atomic ratio	S/(W + Ga) atomic ratio
WS_2	32.2 (45%) 35.5 (55%)	–	161.2	–	0.90
0.5% Ga/WS_2	32.3	1117.8 (100%)	161.3	0.084	1.85
1.5% Ga/WS_2	32.3	1117.8 (85%) 1119.7 (15%)	161.2	0.189 (0.161)[a]	1.98
2.5% Ga/WS_2	32.3	1117.9 (69%) 1119.8 (31%)	161.1	0.342 (0.236)[a]	1.89

[a] Ga_2S_3/W atomic ratio indicating the surface exposure of Ga_2S_3 species.
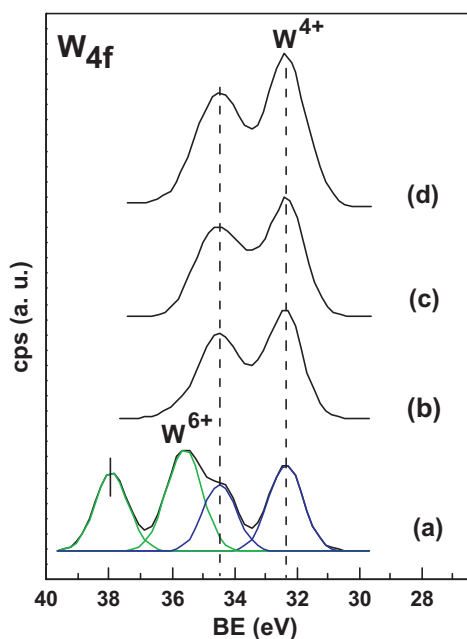
Fig. 3. W 4f core-level spectra of the unsupported catalysts: (a) WS_2, (b) 0.5% Ga/WS_2, (c) 1.5% Ga/WS_2 and (d) 2.5% Ga/WS_2.
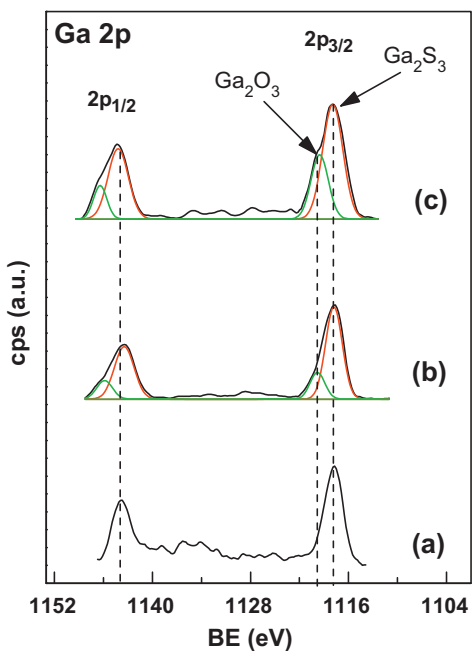
Fig. 4. Ga 2p core-level spectra of the Ga_2S_3/WS_2 catalysts: (a) 0.5% Ga/WS_2, (b) 1.5% Ga/WS_2 and (c) 2.5% Ga/WS_2.

which is characteristic for pure WS_2 phase [23,49–51]. Thus, one might conclude that the addition of gallium onto unsupported WS_2 catalysts led to total sulfidation of the WO_3 species. In good agreement with the ESR spectra of unsupported WS_2 catalysts prepared by the decomposition of thiosalt [52], the XPS measurements precluded the presence of oxo-W^{5+} species in the bulk Ga/WS_2 catalysts.

The Ga 2p$_{3/2}$ spectra for the lower Ga-content sample showed a narrow Ga 3d peak with BE close to 1117.8 eV, which is assigned to sulfided Ga^{3+} species in the Ga_2S_3 phase [53,54]. Contrary to this sample, the medium and high Ga-loaded catalysts showed two peaks at 1119.7 and 1117.8 eV. These BE are assigned to oxidized and sulfided Ga^{3+} species, associated with Ga_2O_3 and Ga_2S_3 phases, respectively [54]. It is noticed that the amount of oxidized Ga species increases with increasing Ga-content, this is in agreement with XRD results. The explanation to this observation could be related with the formation of large Ga particles in medium and high Ga-contents, which are difficult to sulfide under the conditions employed in this work.

As expected, the surface exposure of Ga species increases with an increase of Ga-loading in the samples. Thus, the amount of exposed $Ga^{\delta+}$ ions over W surface is the highest in 2.5% Ga/WS_2 catalyst. The S/(W + Ga) atomic ratios of the catalysts follow the order: 1.5% Ga/WS_2 > 2.5% Ga/WS_2 > 0.5% Ga/WS_2 > WS_2 suggesting easier sulfidation of tungsten species in the presence of $Ga^{\delta+}$ ions. These differences in the sulfidation degree might take place during the complex physicochemical processes occurring during the impregnation followed by sulfidation.

3.4. FTIR of adsorbed CO

It is well established that the active phase of tungsten HDS catalysts is constituted by small nanoparticles of lamellar WS_2 species, in the form of sandwiched S–W–S slabs, stacked on the top of each other and separated by van der Waal's gaps [2]. To understand more deeply the effect of the gallium introduction on the population of edge or corner tungsten sites of the WS_2 crystallites, the FTIR study of CO adsorption at about $-100\,^\circ$C on the freshly sulfided catalysts was performed. The CO-FTIR spectra of CO adsorbed on Ga-free and two Ga-containing catalysts are shown in Fig. 5. All IR-CO spectra showed two principal absorption bands at 2068 and 2110 cm^{-1}. Considering the recent FTIR-CO study on MoS_2 catalysts by Zecchina et al. [55], the IR band at 2070 cm^{-1} is ascribed to CO chemisorbed on the "corner-sites" of the WS_2 crystallites, while the band at 2110 cm^{-1} originates from CO adsorption on the "edge-sites" of those crystallites. As seen in Fig. 5, the intensity of the band at 2070 cm^{-1} follows the trend: 1.5% Ga/WS_2 > 2.5% Ga/WS_2 » WS_2. This trend suggests that the most active 1.5% Ga/WS_2 catalyst shows the largest proportion of "corner-sites" among the catalysts studied. Our results are in good agreement with electron spin resonance analysis of sulfided $GaNiMo/Al_2O_3$ catalysts performed by Park and Rhee [43], which suggested that addition of Ga increases the bulk defects in the MoS_2-like phase or Mo^{3+} ions connected to anion
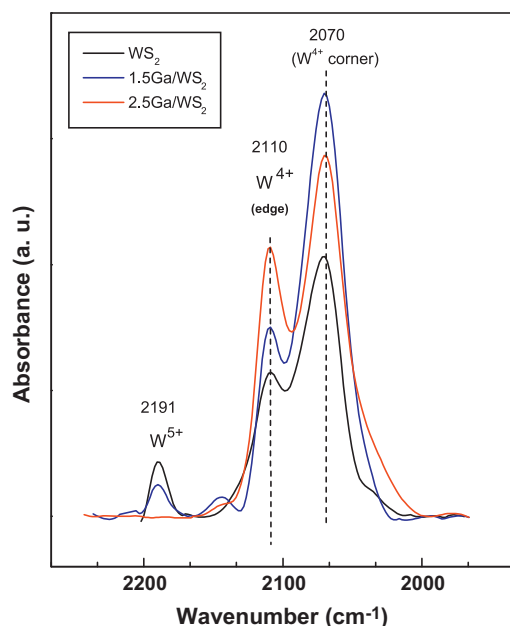
Fig. 5. FTIR spectra of CO adsorbed at about −100 °C on the unsupported WS_2 and Ga_2S_3/WS_2 catalysts.

vacancies, and directly related to the catalytic activity. The influence of CUS sites of the WS_2 phase on the catalyst HDS activity is discussed below.

Additionally, the WS_2 and 1.5% Ga/WS_2 catalysts show an absorption band at about 2191 cm^{-1}. This band does not originate from W^{6+}(CO) species because the CO molecule cannot be adsorbed on W^{6+} ions [56]. Considering the FTIR study of CO adsorption on reduced W/Al_2O_3 [30] and W/SiO_2 catalysts [57], the band at 2191 cm^{-1} can be assigned W^{5+}(CO) species. The absence of this band in the FTIR-CO spectra of 2.5% Ga/WS_2 sample suggests that easier reducibility of tungsten species on this catalyst with respect to WS_2 and 1.5% Ga/WS_2 samples, in good agreement with XRD and XPS data (*vide supra*).

3.5. TPD-NH$_3$

To examine the effect of the Ga incorporation on surface acidity, ammonia TPD measurements were conducted for all sulfided catalysts. Fig. 6 shows the TPD-NH$_3$ profiles of the sulfided Ga/WS_2 catalysts and WS_2 sample. The TPD-NH$_3$ profiles were treated mathematically using Gaussian functions (not shown here). The first peak between 100 and 400 °C can be attributing to ammonia adsorbed on tungsten species [58], which are formed during catalyst pre-treatment under the H_2S/H_2 mixture. The concentrations of those acid sites (expressed as mmol of NH$_3$ desorbed per g of catalyst) are listed in Table 1. As seen in this table, the acidity trend follows the trend: 2.5% Ga/WS_2 > 1.5% Ga/WS_2 > 0.5% Ga/WS_2 ≈ Ga-free sample.

Contrary to the first peak, the interpretation of second peak located at temperature higher than 400 °C is straightforward because some decomposition species of the sulfide phase might be responsible for this high temperature component. Considering previous DTA/TGA study on the thermal decomposition of an ATT precursor in flowing N_2 [59], the ATT precursor is decomposed in two steps:

(1) $(NH_4)_2WS_4 \rightarrow WS_3 + 2NH_3 + H_2S$ (thermal decomposition at about 250 °C)
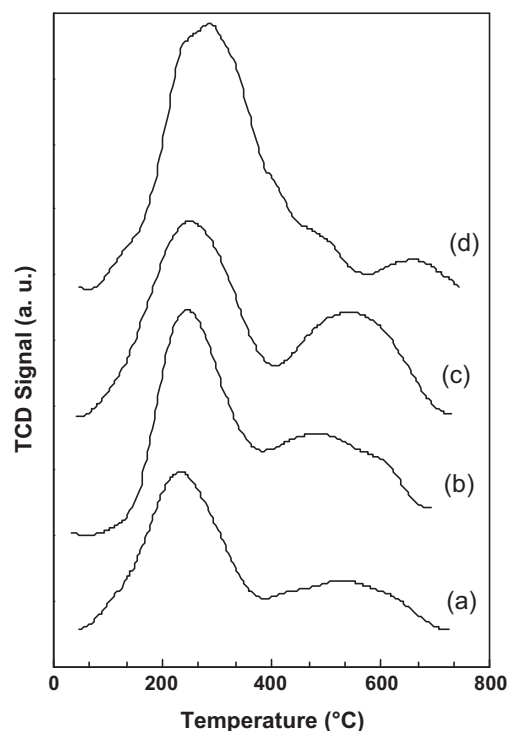(2) $WS_3 \rightarrow WS_2 + S^0$ (thermal decomposition at about 360 °C)

Fig. 6. TPD-NH$_3$ profiles of the unsupported catalysts: (a) WS_2, (b) 0.5%Ga/WS_2, (c) 1.5% Ga/WS_2 and (d) 2.5% Ga/WS_2.

Thus, the second peak in TPD-NH$_3$ profiles could be due not only to the NH$_3$ desorption from medium strength acid sites but also to evolution of some S^0 species retained on the support surface.

3.6. Catalyst activity in HDS of DBT

Investigation of the activity of catalysts can provide information on the catalytic active sites. With this aim, we examined the initial catalytic behavior of all sulfided catalysts in the HDS of DBT reaction carried out in batch reactor at 320 °C under hydrogen pressure of 5.5 MPa. Before activity tests, all catalysts were sulfided at 450 °C for 6 h. The influence of Ga-loading on the initial reaction rate is displayed in Fig. 7. WS_2/Al_2O_3 catalyst (W-loading of 2.8 nm^{-2}) was used as reference. As seen in Fig. 7, all unsupported catalysts showed higher catalytic activity in comparison with the reference sample. The addition of gallium to bulk WS_2 catalyst led to an increase of the catalytic activity with respect to Ga-free
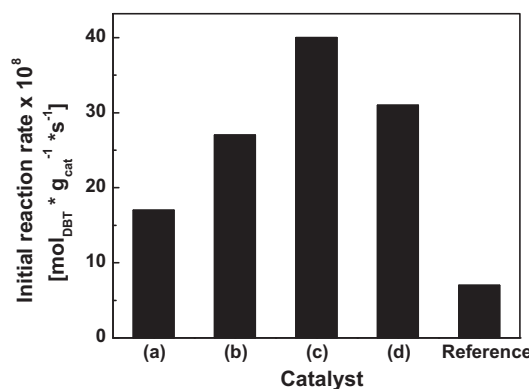

Fig. 7. Initial reaction rate of sulfided catalysts in the HDS of DBT: (a) WS_2, (b) 0.5%Ga/WS_2, (c) 1.5% Ga/WS_2 and (d) 2.5% Ga/WS_2. As reference, the reaction rate of the sulfided W/Al_2O_3 catalyst (W-loading of 2.8 nm^{-2}) has been reported.

Table 3
Selectivities at 40% of DBT conversion in HDS of DBT over bulk WS$_2$ and sulfided Ga/WS$_2$ bulk catalysts.

Catalyst	HYD[a]			DDS[b]	HC[c]		(HYD + HC)/DDS	HYD/DDS
	DCH	CHB	THDBT	BP	BZ	CH		
WS$_2$	4	7	4	85	n.d.	n.d.	0.18	0.18
0.5% Ga/WS$_2$	4	10	5	81	Traces	Traces	0.23	0.23
1.5% Ga/WS$_2$	6	16	4	62	8	4	0.61	0.42
2.5% Ga/WS$_2$	8	18	4	55	10	5	0.82	0.55

n.d., non detected.
[a] Hydrogenation reaction route leading to dicyclohexyl (DCH), cyclohexylbenzene (CHB) and tetrahydrodibenzothiophene (THDBT).
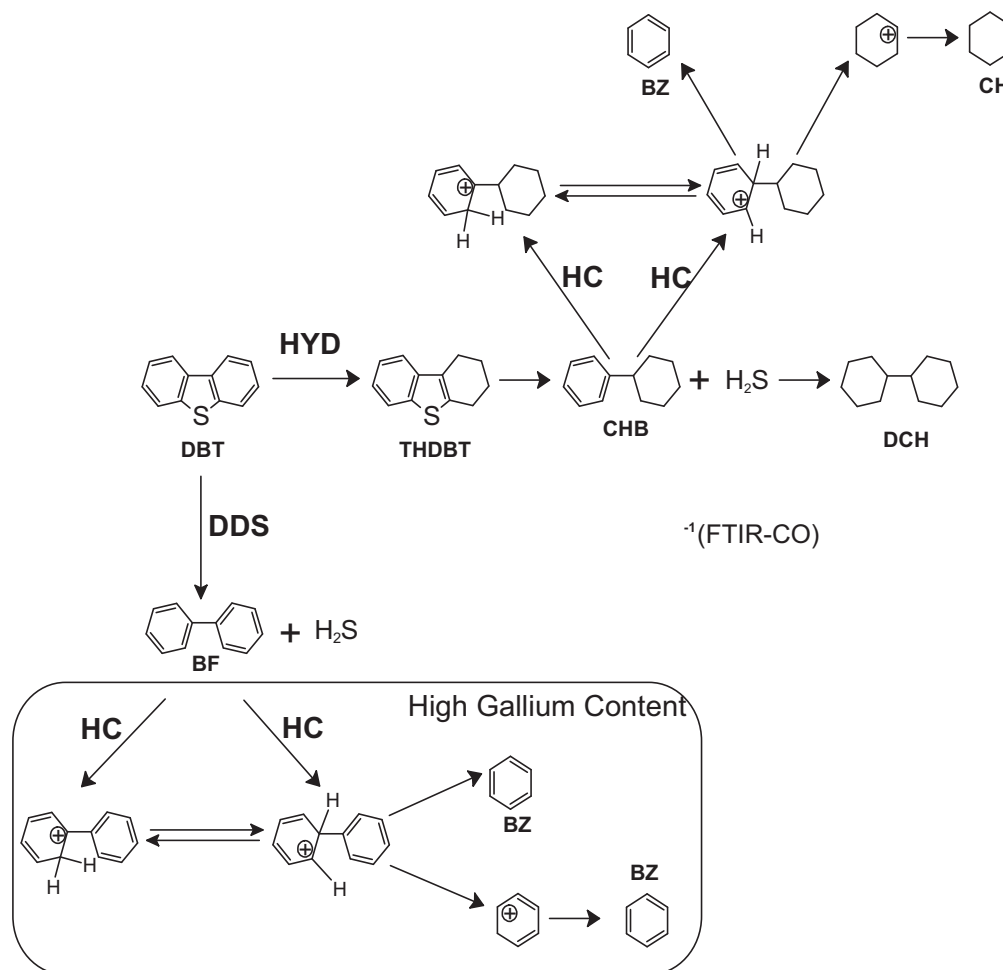[b] Direct desulfurization reaction route leading to biphenyl (BP) formation.
[c] Hydrocracking of DBT leading to benzene (BZ) and cyclohexane (CH).

WS$_2$ sample. The observed activity trend is: 1.5% Ga/WS$_2$ > 2.5% Ga/WS$_2$ > 0.5% Ga/WS$_2$ > WS$_2$ > WS$_2$/Al$_2$O$_3$. As seen in Fig. 7, the reaction rates of the catalysts follow a volcano type-curve, with the 1.5% Ga/WS$_2$ catalysts displaying the largest activity among the catalysts studied. This sample was 2.4 times more active than the Ga-free WS$_2$ sample and 4.2 times more active than the reference WS$_2$/Al$_2$O$_3$ catalyst.

For all catalysts, the products of the HDS of DBT were: biphenyl (BP), 1,2,3,4-tetrahydrodibenzothiophene (THDBT), cyclohexyl-benzene (CHB) and dicyclohexyl (DCH). Additionally, for the both 1.5% Ga/WS$_2$ and 2.5% Ga/WS$_2$ catalysts, benzene (BZ) and cyclohexane (CH) were detected indicating that hydrocracking occurs. The selectivity toward different products, as determined at 40% of DBT conversion and expressed as %, is shown in Table 3. As

seen in this table, the selectivity achieved over Ga-containing catalysts is different from that found on bulk WS$_2$. Scheme 1 shows a tentative reaction pathway based on the products detected. The reaction is proposed to occur according to two parallel routes: direct desulfurization (DDS) and hydrogenation (HYD) [1,2]. The former involves direct S-removal, while the latter involves two steps: hydrogenation of one of the aromatic ring in the first step, followed by S-removal as H$_2$S in the second step [2]. In this "parallel" reaction mechanism, the CHB formation does not rely on the sequential hydrogenation product of biphenyl. Therefore, biphenyl may be classified as a product of C–S bond hydrogenolysis, whereas cyclohexylbenzene is derived from DBT hydrogenation followed by desulfurization. The selectivity results shows in Table 3, clearly indicate that the principal route of the reaction is the

Scheme 1. Reaction scheme for the HDS of DBT over unsupported WS$_2$ and Ga$_2$S$_3$/WS$_2$ catalysts. HYD, hydrogenation; DDS, direct desulfurization; HC, hydrocracking.

direct desulfurization (DDS of 55–85%) leading to formation of biphenyl. The formation of dicyclohexyl, cylohexylbenzene and tetrahydrodibenzothiophene points to the DBT transformation via hydrogenation (HYD) route. It is noteworthy that an increase of gallium content in the binary samples led to the enhancement of the selectivity toward hydrogenation products from 15% (WS_2) to 30% (2.5% Ga/WS_2), while the DDS selectivity decreases. The selectivity toward benzene and cyclohexane increases going from 1.5% Ga/WS_2 to 2.5% Ga/WS_2 sample suggesting that formation of those products is linked with gallium species. This is in good agreement with study by Olorunyolemi and Kydd [42], which performed cumene cracking experiments (in absence of hydrogen) over hybrid gallium–aluminium oxides. Because pure alumina was not active in this reaction and the rate of cumene conversion increased as gallium content increased, it was concluded that the presence of gallium in the hybrid material introduces an acid function [42], in good agreement with our TPD-NH_3 data (*vide infra*). Table 3 lists HYD/DBT and (HYD + HC)/DDS selectivity ratios calculated at 40% of DBT conversion. As seen in this table, those both parameters increase with an increase of gallium loading in the catalysts.

Summarizing, on the basis of the catalyst activity results, the following important observations can be made on the effect of Ga incorporation onto unsupported WS_2 catalysts: (i) enhancement of catalytic activity with respect to WS_2 sample; (ii) enhancement of HYD route of DBT HDS transformation with simultaneous decrease of DDS route of this reaction; (iii) starting of hydrocracking reactions of aromatics rings on the two catalysts with the largest Ga-content (1.5 and 2.5 wt%); (iv) the volcano-curve trend of activity indicated that Ga content has to be optimized, and (v) the 1.5% Ga/WS_2 catalyst shows the largest activity among the catalysts studied as derived from Fig. 7, the largest activity of the 1.5% Ga/WS_2 sample is due to the optimal value of Ga/W atomic ratio. Our bulk Ga/WS_2 catalysts displayed similar volcano-curve activity trend as that reported for WS_2 catalysts supported on alumina modified with Ga, which were tested in HDS of DBT upon similar reaction conditions (batch reactor, $T = 320\,°C$, $P = 5.0\,MPa$) [41]. For the WS_2/Ga–Al_2O_3 catalysts [41], the optimum Ga loading was found to be 1.09 wt% of Ga, which is close to 1.5 wt% of our most active 1.5% Ga/WS_2 catalyst. The comparison of the initial reaction rates indicated that our bulk 1.5% Ga/WS_2 catalyst is 10-times more active than the $WS_2/Ga(1.09)$–Al_2O_3 sample [41]. Thus, we can conclude that bulk Ga_2S_3/WS_2 catalyst is more promising for HDS reaction than its alumina-supported WS_2 counterpart.

3.7. Catalyst activity–structure correlation

Both freshly sulfided 1.5% Ga/WS_2 and 2.5% Ga/WS_2 catalysts possess both Ga_2O_3 and Ga_2S_3 types of clusters decorating the surface of the WS_2 substrate, as demonstrated by XRD and XPS. The Ga_2S_3 is a stable gallium sulfide phase [60], as it was confirmed previously by temperature-programmed reduction analysis of a bulk commercial α-Ga_2S_3 catalyst [39]. In general, the incorporation of gallium on the bulk WS_2 catalyst led to: (i) development of small pores with parallel increase of specific BET surface area and pore volume with respect to the Ga-free WS_2 sample; (ii) decrease of the particle size of WS_2 crystallites formed upon catalyst sulfidation at 450 °C (from XRD); (iii) enhancement of the sulfidation degree of tungsten species (from XPS and FTIR-CO); (iv) increase of the catalyst acidity, as confirmed by TPD-NH_3; and (v) creation of a larger amount of coordinatively unsaturated sites (CUS), as derived by FTIR-CO measurements. As a consequence, this study demonstrated that the presence of the Ga_2S_3 species on the surface of bulk WS_2 catalyst improves both the activity and selectivity of DBT HDS reaction. Similarly, when gallium was added as a second promoter to $NiMo/Al_2O_3$ catalyst, a substantial increase in the HDN conversion of pyridine was observed by Park and Rhee [43].
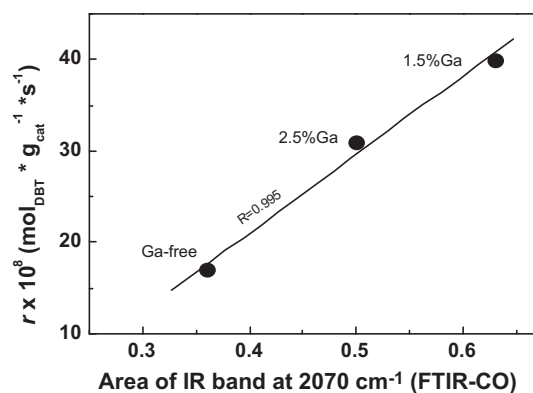

Fig. 8. Influence of the "corner sites" of WS_2 species on the catalyst activity.

Considering small gallium loading (0.5–2.5 wt%), the contribution of gallium species to the catalyst HDS activity is very low, if any. Indeed, it was reported that Ga_2S_3/Al_2O_3 catalyst showed a very low HDN conversion at 400 °C and hydrogen pressure of 3.5 MPa [43]. Thus, the catalyst activity results could be explained considering the role of gallium as promoter and/or by modification of the catalyst morphology induced by gallium.

The reasons why the addition of gallium onto WS_2 catalyst enhances the catalyst activity can be explained considering the observed catalyst structure–activity correlations. From the combined FTIR-CO and TPD-NH_3 results, it is clear that Ga incorporation facilies the formation of anion vacancies and acid sites on the sulfide phases. As a consequence, the HDS reaction mechanism is bifunctional for all catalysts: the reduced tungsten sites dissociate hydrogen molecules and perform the hydrogenation whereas the acidic sites allow the removal of sulfur atom by direct desulfurization reaction pathway. In particular, the hydrocracking in the HDS reaction over 1.5% Ga/WS_2 and 2.5% Ga/WS_2 catalysts could be explained considering the presence of the Ga_3O_3 species decorating surfaces of both samples. Thus, for those catalysts the hydrocracking is linked with the presence of Lewis Ga^{3+} acid sites, which shows the preference for C–H activation, as it was demonstrated by cracking of *n*-heptane over gallium-containing ZSM-5 zeolites [61].

It was found a linear correlation between the catalyst activity and area of the IR band at 2070 cm^{-1} indicating amount of WS_2 "corner sites" (Fig. 8). This correlation suggests that the enhancement of the activity of Ga-containing catalysts in the HDS DBT reaction is linked to an increase in the number of active sites (CUS) of the tungsten sulfide caused by presence of gallium species decorating the surface of the WS_2. Thus, the largest activity of the 1.5% Ga/WS_2 sample could be explained considering its largest amount of CUS sites among the catalysts studied, the largest sulfidation degree (from XPS) and moderate acidity (Table 1) diminishing the coke formation during HDS reaction.

Considering the factors influencing on the selectivity in the HDS of DBT reaction, it was found that the intensity of the IR band at 2110 cm^{-1} corresponding to CO adsorbed on W^{4+} edge sites (Fig. 5) follows the same trend as the HYD/DDS selectivity ratio (Table 3). Thus, in good agreement with Ref. [43], the increase of edge sites induced by gallium gives rise to the favorable effect on the DBT transformation route via hydrogenation pathway. Similarly to the catalyst activity, the selectivity toward HYD + HC products increases linearly with an increase of the catalyst acidity, as shown in Fig. 9(a). This is because an increase of the catalyst acidity facilitates the ring saturation ability and further cracking of C–C bonds [62]. The enhancement of hydrogenation route of HDS reaction increased also with an increase of the surface exposure of Ga_2S_3 species, as it is inferred from
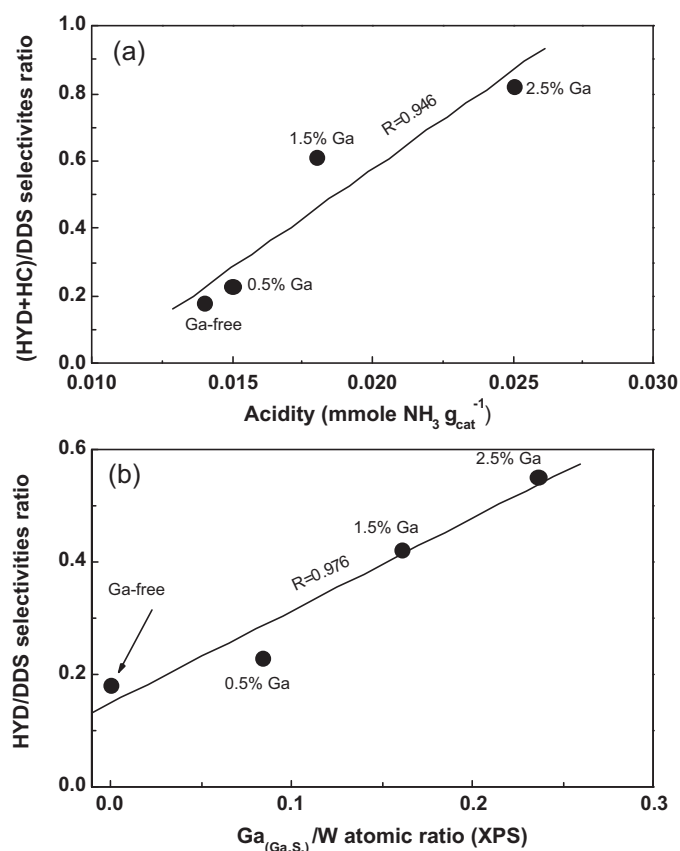
Fig. 9. (a) Influence of the catalyst acidity on the (HYD + HC)/DDS selectivities ratio. (b) Correlation between the surface exposure of Ga_2S_3 species and the HYD/DDS selectivities ratio.

Fig. 9(b) which show a linear correlation between the HYD/DDS selectivities ratio and the Ga/W atomic ratio corresponding to the Ga_2S_3 phase (from XPS). This correlation suggests that the enhancement of HYD reaction over sulfided Ga/WS$_2$ catalysts can be due to participation of Ga_2S_3 species in HYD reaction mechanism. The enhancement of hydrogenation activity was reported previously for GaNiMo/Al$_2$O$_3$ catalysts tested in HDN of pyridine [43] and the high affinity of gallium species to hydrogen was confirmed by hydrogen–TPD analysis of the gallium-containing hybrid catalysts [63].

4. Conclusions

The incorporation of Ga into WS$_2$ catalysts have multiple and complex effects on the morphology of sulfided unsupported Ga/WS$_2$ systems. Gallium incorporation on the base WS$_2$ catalyst enhanced the HYD route of HDS of DBT reaction. This was linked with an increase of catalyst acidity, the enhancement of the catalyst sulfidation degree, and more favorable morphology of WS$_2$ crystallites having a larger amount of CUS sites. The performance of the HDS catalysts was explained from the viewpoint of dual catalyst functionality.

Acknowledgements

References

[1] P.T. Vasudevan, J.L.G. Fierro, Catal. Rev. Sci. Eng. 38 (1996) 161–188.
[2] B. Pawelec, R.M. Navarro, J.M. Campos-Martin, J.L.G. Fierro, Catal. Sci. Technol. 1 (2011) 23–42.
[3] H. EP Directive 2003/17/EC, Office J. Eur. Union L76, 46 (2003) 10.
[4] T.A. Zepeda, Appl. Catal. A: Gen. 347 (2008) 148–161.
[5] K.G. Knudsen, B.H. Cooper, H. Topsøe, Appl. Catal. A: Gen. 189 (1999) 205–215.
[6] D.D. Whitehurst, T. Isoda, I. Mochida, Adv. Catal. 42 (1998) 345–471.
[7] I.V. Babich, J.A. Moulijn, Fuel 82 (2003) 607–631.
[8] C. Song, Catal. Today 86 (2003) 211–263.
[9] B. Pawelec, P. Castaño, T.A. Zepeda, Appl. Surf. Sci. 254 (13) (2008) 4092–4102.
[10] R. Nava, J. Morales, G. Alonso, C. Ornelas, B. Pawelec, J.L.G. Fierro, Appl. Catal. A: Gen. 321 (2007) 58–70.
[11] B. Pawelec, R.M. Navarro, J.M. Campos-Martin, A. López-Agudo, P.T. Vasudevan, J.L.G. Fierro, Catal. Today 886 (2003) 73–85.
[12] J.A. Anderson, B. Pawelec, J.L.G. Fierro, P.L. Arias, F. Duque, J.F. Cambra, Appl. Catal. A: Gen. 99 (1993) 55–70.
[13] R. Iwamoto, J. Grimblot, Adv. Catal. 44 (2000) 417–503.
[14] T.A. Zepeda, B. Pawelec, J.L.G. Fierro, A. Montesinos, A. Olivas, S. Fuentes, T. Halachev, Micropor. Mesopor. Mater 111 (1–3) (2008) 493–506.
[15] S.L. Soled, S. Miseo, R. Krikak, H. Vroman, T.H. Ho, K.L. Riley, US Patent, 6,299,760 B1 (2001).
[16] G. Alonso, M.H. Siadati, G. Berhault, A. Aguilar, S. Fuentes, R.R. Chianelli, J. Catal. 208 (2002) 359–369.
[17] R. Huriache-Acuña, M.A. Albiter, J. Espino, C. Ornelas, G. Alonso-Nuñez, F. Paraguay-Delgado, J.L. Rico, R. Martínez-Sánchez, Appl. Catal. A: Gen. 304 (2006) 124–130.
[18] K. Ramanathan, S.W. Weller, J. Catal. 95 (1985) 249–259.
[19] H. Hoshi, H. Hayashi, Toyota Tech. Rev. 53 (2004) 10–15.
[20] F.L. Plantenga, R. Cefortain, S. Eijsbouts, F. Van Houtert, G.H. Anderson, S. Miseo, S. Soled, K. Riley, K. Fujita, Y. Inoue, Stud. Surf. Sci. Catal. 145 (2003) 407–410.
[21] R.I. Walton, A.J. Dent, S.J. Hibble, Chem. Mater. 10 (11) (1998) 3737–3745.
[22] K. Wilkinson, M.D. Merchán, P.T. Vasudevan, J. Catal. 171 (1997) 325–328.
[23] B. Pawelec, R. Navarro, J.L.G. Fierro, P.T. Vasudevan, Appl. Catal. A: Gen. 168 (1998) 205–217.
[24] J.A. Lumbreras, R. Huirache-Acuña, E.M. Rivera-Muñoz, G. Berhault, G. Alonso-Núñez, Catal. Lett. 134 (2010) 138–146.
[25] D. Zuo, M. Vrinat, H. Nie, F. Mauge, Y. Shi, M. Lacroix, D. Li, Catal. Today 93–95 (2004) 751–760.
[26] S. Zeng, J. Blanchard, M. Breysse, Y. Shi, X. Su, H. Nie, D. Li, Appl. Catal. A: Gen. 294 (2005) 59–67.
[27] P. Afanasiev, M. Cattenot, C. Geantet, N. Matsubayashi, K. Sato, S. Shimada, Appl. Catal. A: Gen. 237 (2002) 227–237.
[28] Y. Ji, P. Afanasiev, M. Vrinat, W. Li, C. Li, Appl. Catal. A: Gen. 257 (2004) 157–164.
[29] B. Pawelec, R. Mariscal, J.L.G. Fierro, A. Greenwood, P.T. Vasudevan, Appl. Catal. A: Gen. 206 (2001) 295–307.
[30] Y. Yan, Q. Xin, S. Jiang, X. Guo, J. Catal. 131 (1991) 234–242.
[31] R. Thomas, E.M. van Oers, V.H.J. de Beer, J. Medema, J. Moulijn, J. Catal. 76 (1982) 241–253.
[32] F. Pedraza, S. Fuentes, Catal. Lett. 65 (2000) 107–113.
[33] F. Maugé, A. Vallet, J. Bachelier, J.C. Duchet, J.C. Lavalley, Catal. Lett. 2 (1989) 57–62.
[34] Y. Okamoto, S. Ishihara, M. Kawano, M. Satoh, T. Kubota, J. Catal. 217 (2003) 12–22.
[35] H. Farag, D.D. Whitehurst, K. Sakanishi, I. Mochida, Catal. Today 50 (1999) 9–17.
[36] T.K.T. Ninh, L. Massin, D. Laurenti, M. Vrinat, Appl. Catal. A: Gen. 407 (2011) 29–39.
[37] A. Cimino, M. Lo Jacono, M. Schiavello, J. Phys. Chem. 79 (3) (1975) 243–249.
[38] M. Lo Jacono, M. Schiavello, V.H.J. De Beer, G. Minelli, J. Phys. Chem. 81 (16) (1977) 1583–1588.
[39] E. Altamirano, J.A. de los Reyes, F. Murrieta, M. Vrinat, J. Catal. 235 (2005) 403–412.
[40] E. Altamirano, J.A. de los Reyes, F. Murrieta, M. Vrinat, Catal. Today 133–135 (2008) 292–298.
[41] J.N. Díaz de León, M. Picquart, M. Villarroel, M. Vrinat, F.J. Gil Llambias, F. Murrieta, J.A. de los Reyes, J. Mol. Catal. A: Chem. 323 (1–2) (2010) 1–6.
[42] T. Olorunyolemi, R. Kydd, J. Catal. 158 (1996) 583–586.
[43] Y.C. Park, H.K. Rhee, Appl. Catal. A 179 (1999) 145–153.
[44] A. Olivas, T.A. Zepeda, I. Villalpando, S. Fuentes, Catal. Commun. 9 (6) (2008) 1317–1328.
[45] Y.Q. Zhu, W.K. Hsu, N. Grobert, B.H. Chang, M. Terrones, H. Terrones, H.W. Kroto, D.R.M. Walton, Chem. Mater. 12 (2000) 1190–1194.
[46] C. Komatsu-Hidaka, T. Takizawa, J. Cryst. Growth 222 (3) (2001) 574–578.
[47] Y. Su, Mi Gao, X. Meng, Y. Chen, Q. Zhou, L. Li, Yi Feng, J. Phys. Chem. Solids 70 (7) (2009) 1062–1065.
[48] A. Montesinos-Castellanos, T.A. Zepeda, Micropor. Mesopor. Mater. 113 (1–3) (2008) 146–162.
[49] A. Benítez, J. Ramírez, J.L.G. Fierro, A. López Agudo, Appl. Catal. A: Gen. 144 (1996) 343–364.
[50] M. Breysse, M. Cattenot, T. Decamp, R. Frety, C. Gachet, M. Lacroix, C. Leclerq, L. de Mourgues, J.L. Portefaix, M. Vrinat, M. Houari, J. Grimblot, S. Kasztelan, J.P. Bonnelle, Catal. Today 4 (1988) 39–55.
[51] B. Pawelec, S. Damyanova, R. Mariscal, J.L.G. Fierro, I. Sobrados, J. Sanz, L. Petrov, J. Catal. 223 (2004) 86–97.

[52] A.J.A. Konings, A.M. van Dooren, D.C. Koningsberger, V.H.J. de Beer, A.L. Far-ragher, G.C.A. Schuit, J. Catal. 54 (1978) 1–12.

[53] M.R. Lazell, P.O. Brien, D.J. Otway, J.-H. Park, Chem. Mater. 11 (12) (1999) 3430–3432.

[54] P.N. Lisboa-Filho, V.R. Mastelaro, W.H. Schreiner, S.H. Messaddeq, M. Siu Li, Y. Messaddeq, P. Hammer, S.J.L. Ribeiro, P. Parent, C. Laffon, Solid State Ionics 176 (2005) 1403–1409.

[55] F. Cesano, S. Bertarione, A. Piovano, G. Agostini, M. Mastabur Rahman, E. Groppo, F. Bonino, D. Scarano, C. Lamberti, S. Bordiga, L. Montanari, L. Bonoldi, R. Millini, A. Zecchina, Catal. Sci. Technol. 1 (2011) 123–136.

[56] J.L.G. Fierro, in: J.L.G. Fierro (Ed.), Spectroscopic Characterization of Heteroge-neous Catalysts. Part B: Chemisorption of Probe Molecules, vol. 57, Elsevier, Amsterdam, 1990, p. B121.

[57] S.D. Kohler, J.G. Ekerdt, J. Phys. Chem. 98 (1994) 1276–1281.

[58] B. Jarry, F. Launay, J.P. Nogier, V. Montouillout, L. Gengembre, J.L. Bonardet, Appl. Catal. A: Gen. 309 (2006) 177–186.

[59] J. Espino, L. Alvarez, C. Ornelas, J.L. Rico, S. Fuentes, G. Berhoult, G. Alonso, Catal. Lett. 90 (2003) 71–79.

[60] F. Hulliger, in: F. Levy (Ed.), Physics and Chemistry of Materials with Layered Structures, Structural Chemistry of Layered-type Phases, vol. 5, Reidel, Dor-drecht, 1976, p. 183.

[61] N. Rane, M. Kersbulck, R.A. van Santen, E.J.M. Hensen, Micropor. Mesopor. Mater. 110 (2008) 279–291.

[62] (a) A. Olivas, T.A. Zepeda, Catal. Today 143 (2009) 120–125;
(b) B. Pawelec, T. Halachev, A. Olivas, T.A. Zepeda, Appl. Catal. A: Gen. 348 (1) (2008) 30–41.

[63] R. Carli, R. Le Van Mao, C.L. Bianchi, V. Ragaini, Catal. Lett. 21 (1993) 265–274.